Synthesis of TiC and SiC/TiC nanocrystalline powders by gas-phase laser-induced reaction

R. ALEXANDRESCU
Institute of Atomic Physics, Laser Department, P.O. Box MG6, Bucharest, Romania
E. BORSELLA, S. BOTTI, M. C. CESILE, S. MARTELLI
ENEA Innovation Department, Applied Physics Division, P.O. Box 65, 00044 Frascati, Italy
R. GIORGI, S. TURTÙ, G. ZAPPA
ENEA Innovation Department, New Materials Division, P.O. Box 2400, 00100 Rome, Italy

In the development of advanced ceramic nanocomposites, the production of titanium-based nanopowders has assumed importance, especially since recent results showed that mechanical properties of SiC matrices could be significantly improved by the incorporation of TiC second phase and vice versa. Nanosized TiC and TiC/SiC powders were synthesized by CO_2 laser-induced reactions. A $TiCl_4$ and hydrocarbons mixture was irradiated for titanium carbide production; the addition of SiH_4 gave rise to the composite powders. The results of the powder characterization, obtained mainly by X-ray photoelectron spectroscopy, X-ray-induced Auger Spectroscopy and X-ray diffraction, are discussed in detail to correlate the reaction parameters to the composition and morphology of the products. Both TiC and SiC/TiC nanopowders showed a high reactivity to the air exposure, as evinced by the surface oxidation of the particles. Nevertheless, a quite good yield was obtained for nanocomposites of β-SiC matrix with the addition of up to 20% TiC phase.

1. Introduction

The demand for advanced ceramic materials has stimulated increasing interest in producing nanocrystalline ceramic powders, because, starting from nanosized particles, typical drawbacks of traditional ceramics, such as negligible ductility, high-temperature processing and large internal flaws, could be reduced. Moreover, the research for ultrafine-grained powder production has assumed further importance, especially because it has been reported that the performances of reinforced composite materials can be greatly improved when the size of the reinforcing component is reduced to nanometre scale [1].

Titanium carbide (TiC) is a very attractive material for its quite high hardness (H_v: 3200), arising from the high degree of covalent bonding brought about by the carbon contribution to the bond strength [2]. It combines a very high refractoriness (melting point $> 3000\,^{\circ}C$) and thermal stability with excellent wear resistance, low friction coefficient and considerable thermal and electrical conductivity, but some limits of its application under severe stress are due to its low sinterability and toughness.

Among structural ceramics, silicon carbide (SiC) deserves particular attention for its high strength and wear resistance at elevated temperatures, but it exhibits poor reliability, owing to the intrinsic brittleness and low fracture toughness in the monolithic state. Furthermore inherent brittleness and high hardness produce difficulties in machining SiC due to chipping, thus contributing to the high cost of such a ceramic [3].

Recently SiC/TiC composites were investigated to overcome the above-mentioned difficulties. On one side the dispersion of fine SiC particles into TiC matrices showed an increasing in the fracture strength in hot-pressed monolithic samples (up to 820 MPa); furthermore the toughness value was raised from 3.5 MPa $m^{1/2}$ to 4.4 MPa $m^{1/2}$ and this behaviour was attributed to the refinement of the SiC matrix by SiC particle addition [4]. On the other hand, TiC addition to SiC matrices proved that for SiC/TiC composite, the density of the sintered body increased abruptly with up 25 wt % TiC content. At the same time it was shown that the flexural strength in SiC/TiC hot-pressed composites, measured at room temperature at 1500 °C could be increased from about 300 MPa for the SiC sample, up to 920 MPa (at 1500 °C) by 30 wt % TiC addition [5].

The mechanical properties of these composites are expected to improve when the structure of the constituents is reduced to nanometric scale, producing homogeneous and intimate mixtures of nanophases.

In this area, the CO_2 laser-induced pyrolysis of gaseous reactants has proved a viable system to produce nanoscale ultrapure silicon-based ceramic powders, as SiC and Si_3N_4 as well as SiC/Si_3N_4 nanocomposite powders [6–10], showing superior sintering ability. To our knowledge, few contributions on the production of nanosized TiC and

0022–2461

nano-nanocomposite SiC/TiC particles have been published until now [11–13], most of them concerning synthesis routes different from laser-induced reaction of gaseous precursors and mainly related to microelectronics applications.

The aim of this paper is to show that laser pyrolysis is a suitable method for TiC and SiC/TiC synthesis, and to discuss the main process parameters affecting chemical properties and structure of these nanopowders.

2. Experimental procedure

The experimental apparatus for laser synthesis has already been described in detail [9, 10]. Here only the main features are summarized. A CO_2 continuous wave (c.w.) laser (ELEN Mod. 2000, maximum power 1.2 kW) was focused at the centre of the reaction chamber, where it orthogonally intersected the reactant gases mixture which entered the cell through a stainless steel nozzle. A coaxial argon stream (2.5–3.5 standard l min^{-1}) was used to keep the particles entrained in the gas stream to the cell exit.

The gas flow rates were independently controlled by mass flow controllers, while the cell pressure, read on a baratron capacitance, was varied from 300–600 torr (1 torr = 133.322 Pa), and maintained at a constant value during the process by use of a pressure-regulating valve. The temperature of the reaction flame was measured by an optical pyrometer. Nucleated particles were collected in a removable glass tank.

For TiC powder synthesis, liquid titanium tetrachloride ($TiCl_4$) and different hydrocarbons, methane (CH_4), acetylene (C_2H_2) and ethylene (C_2H_4) were employed as gas-phase reactants; for the synthesis of SiC/TiC nanocomposite powders, silane (SiH_4), $TiCl_4$ and, alternatively, C_2H_2 or C_2H_4 were used. Titanium tetrachloride was chosen for its well-known suitability as titanium precursor, due to its low dissociation temperature (500 °C) [14] and a reasonable vapour pressure at room temperature (8 torr at 20 °C) which enables an easy vaporization of the liquid and the vapour transfer into the reaction chamber by a carrier gas. Different $TiCl_4$ and SiH_4 flows corresponding to different SiC/TiC compositions of the final synthesized powders were obtained by heating the $TiCl_4$ liquid at increasing temperature (from 50–90 °C) in a thermostatically-controlled stainless steel bottle. Controlled flows of argon or C_2H_4 were bubbled in the $TiCl_4$ bottle to carry the vapour into the reaction zone.

For TiC production, ethylene gas was always added to the reactant inlet flows to activate and sustain the laser-induced reaction, because of its resonant absorption at the CO_2 laser emission wavelength (10.6 μm). In fact, neither titanium tetrachloride nor the other hydrocarbons could be heated by the CO_2 laser radiation. Ethylene was expected to participate only as heat-exchanging species without being involved in the reaction itself, owing to its higher dissociation energy ($D(H_2C{-}CH_2) = 7.2$ eV) compared with methane and acetylene ($D(2H{-}H) = 4.9$ eV). In the case of SiC/TiC composite powders, silane acted both as sensitizer of the reaction and silicon donor for its strong CO_2 laser radiation absorption. Infrared (IR) spectrophotometry and mass spectrometry (MS) were used as on-line diagnostic to monitor the residual gas composition. With MS analysis, the concentration of reactants and produced gases was estimated by comparing their characteristic ion-peak intensities to the Ar^+ peak (at 40 m/e). In each run, the partial pressures of the exhausted gases (stored down-stream, in a fitted cell) were derived from the IR transmission spectra, by comparing the absorbencies at selected wave numbers ($A = 1/T$, where T is the transmission) with etalon measurements (separately performed for each hydrocarbon, either precursor or gas product). The depletion of $TiCl_4$ vapour, which readily condensed on the cold chamber, walls, was indirectly observed by monitoring the formation of HCl, in the case of TiC, and of various chlorosilanes, in the case of composite SiC/TiC.

Structural, chemical and morphological properties of the produced powders were studied by X-ray diffraction (XRD), X-ray photoelectron and X-ray induced Auger spectroscopy (XPS and XAES) chemical analysis and transmission electron microscopy (TEM).

XPS and XAES measurements were performed using a V.G. Escalab MKII Spectrometer: photoemission peaks Si 2p, C 1s, O 1s, Ti 2p were excited by the unmonochromatized Al$K\alpha$ radiation; Si KLL Auger transition by the bremsstrahlung radiation. XPS quantitative analysis was carried out dividing photoelectron peak areas for sensitivity factors after subtraction of a linear background. A curve-fitting routine, based on the assumption of gaussian peaks, was applied for the decomposition of photoemission peaks.

3. Results and discussion

3.1. TiC synthesis

TiC laser-synthesized powders were ultrafine and dark grey in colour. In Table I the parameters for TiC synthesis and the powder yield are presented. The depletion of each reactant, expressed by the ratio between the final and the initial partial pressures, may be followed as well. It can be noticed that, contrary to what was expected, CH_4 decomposition remained low, while ethylene, the more stable hydrocarbon species, underwent strong dissociation, particularly at high reaction pressures and reaction temperatures (more than 80% in run 4). The high-temperature C_2H_4 pyrolysis was acting as a main source not only of the prevailing content in acetylene by-product found in the exhausted gases, but also of a carbon contamination in the powders. It is worth mentioning that the oxidizing character of chlorine molecules released from $TiCl_4$ generated an outstanding oxidizing environment, thus favouring the high C_2H_4 dissociation yield.

The XRD pattern of all the powders exhibited only the characteristic features of stoichiometric TiC (see Fig. 1), but the XPS quantitative analysis revealed that surface contamination of powders by carbon may reach around 80 at %. The decomposition of the C 1s

TABLE I Experimental parameters for TiC powder formation

Run	$TiCl_4$ (standard $cm^3\ min^{-1}$)	C_2H_4 (standard $cm^3\ min^{-1}$)	CH_4 (standard $cm^3\ min^{-1}$)	C_2H_2 (standard $cm^3\ min^{-1}$)	P (torr)	T (°C)	Yeld ($g\ h^{-1}$)	$\frac{[C_2H_4]_f}{[C_2H_4]_i}$	$\frac{[CH_4]_f}{[CH_4]_i}$	$\frac{[C_2H_2]_f}{[C_2H_4]_i}$	$\frac{[C_2H_2]_f}{[C_2H_2]_i}$
0	12	200	–	12	400	930	1.5	0.70	–	0.20	2.7
1	18	200	–	20	400	970	2.4	0.55	–	0.32	3.2
2	39	200	100	–	500	950	1.6	0.66	0.87	0.27	–
3	45	250	20	–	450	920	1.2	0.58	0.93	0.25	
4	52	200	20	–	600	1200	5.5	0.18	0.75	0.41	–
8	52	150	–	–	400	960	1.8	0.72		0.28	

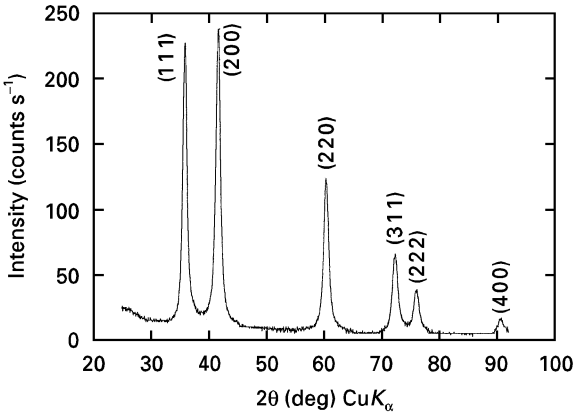

Figure 1 X-ray diffraction pattern of a TiC powder.

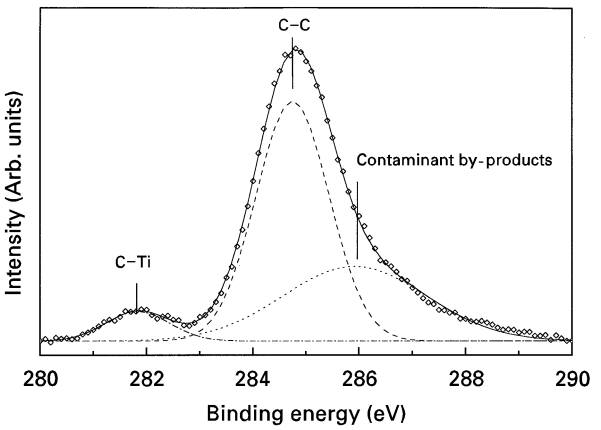

Figure 2 Decomposition of the C 1s photoemission peak of the TiC powder (run 0).

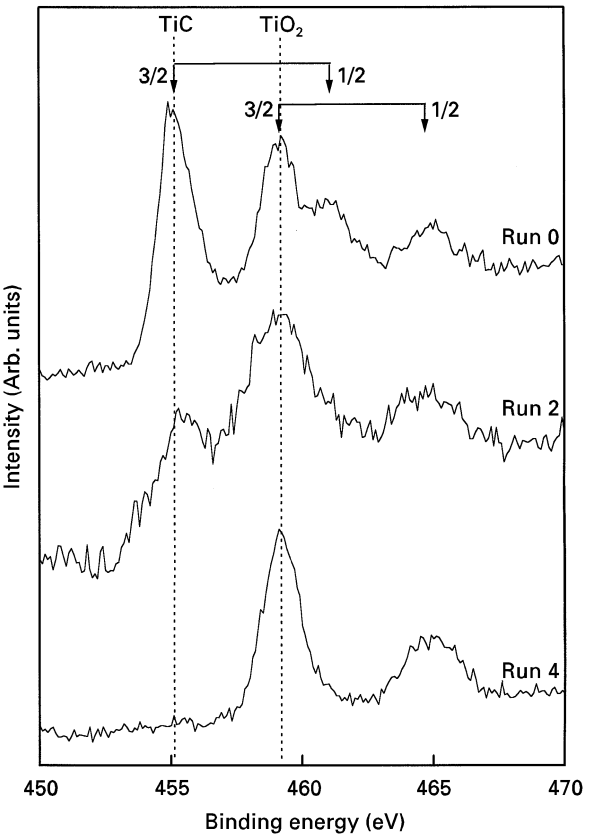

Figure 3 Ti 2p photoemission spectra of TiC powders corresponding to runs 0.2 and 4. The spin-orbit doublet (Ti 2p 3/2, 1/2) is evinced for the TiC and TiO_2 signals.

peak, reported in Fig. 2 for sample 0, showed that only a small fraction of the total carbon could be ascribed to the C–Ti bond, whilst the main component was assigned to the unreacted state and contaminant by-products of the reaction. XPS Ti 2p photoemission spectra also showed that the powders had different degrees of oxidation which could be related to the flame temperature, as shown in Fig. 3 for samples 0, 2 and 4. Furthermore TEM analysis, see Fig. 4, evinced layered spherical particles of 30 nm mean diameter, with a core, whose diffraction pattern corresponded to TiC, whereas the outer layer appeared amorphous. All these findings pointed to a spherical particle structure consisting of a TiC core and an outer oxide layer. This surface oxidation was not so

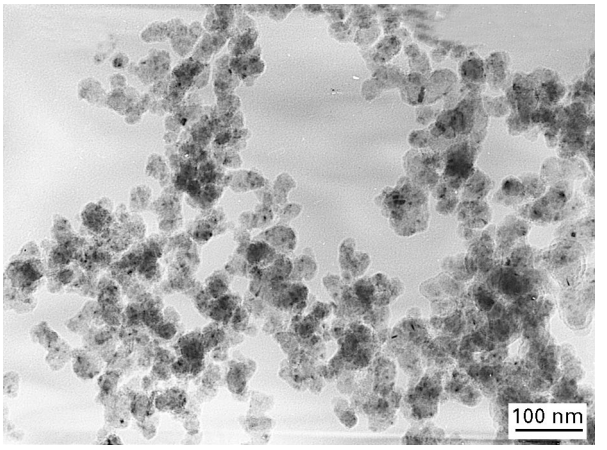

Figure 4 Typical transmission electron micrograph of TiC powders.

surprising, owing to the high reactivity of titanium and titanium carbide with oxygen and considering that the synthesized powders were handled and stored in air. On the other hand, XRD did not show the presence in the diffraction patterns of any reflection peaks, which could be ascribed to known crystalline titanium oxides such as TiO_2 or TiO. The apparent contradiction between XPS and XRD results suggested, together with the transmission electron micrographs, that the outer layer was constituted by an amorphous non-stoichiometric oxide, probably containing carbon atoms (TiC_xO_y).

Powders obtained at the lowest cell pressure and reaction temperatures showed the slightest degree of surface oxidation and free-carbon contamination. A relationship between carbon contamination and oxygen up-take was observed both in TiC and SiC/TiC powders (see below). Chemical analysis of the constituents of TiC powders (one for all, sample 1: 56.7 wt % Ti, 29.2 wt % C and 14.4 wt % O) indicated a relevant amount of oxygen contamination, suggested by the complex envelope of the Ti 2p photoemission peak. These spectra, as shown by the decomposition curve reported in Fig. 5 for sample 0, provided evidence that titanium atoms were engaged with carbon and oxygen not merely in the stoichiometric compounds, but a third component, inclusive of other mixed oxidation states and/or carboxides, had to be considered to reproduce fully the whole envelope, enlightening the complex oxidation processes upon air exposure. Nevertheless, it is worth noting that calcining at moderate temperature (4 h at 600 °C) lead to the complete transformation of the powder into rutile and anatase TiO_2 oxides, with a net weight loss of about 70%, confirming the extremely high reactivity of the nanopowder with oxygen and the large amount of unreacted carbon.

The mechanism leading to different amounts of unreacted carbon in TiC powders deserves further attention. At higher pressures the collision energy transfer processes from excited ethylene towards $TiCl_4$ molecules become more efficient, with the reaction temperature increasing: $TiCl_4$ dissociates first, due to its low thermal activation energy. $TiCl_4$ fragments contribute to a fast dehydrogenation of C_2H_4, both by the oxidizing chlorine atmosphere to which they give rise, and by the known catalytic decomposition over the metallic surface of nascent titanium atoms. Owing to the high carbon affinity of titanium, TiC should be readily formed in high-temperature reactions involving titanium and carbon atoms; at the same time, the huge amount of carbon particles released in the reaction zone by hydrocarbon decomposition further enhances the absorption of the IR radiation, sustaining the high reaction temperatures and the fast dissociation of newly fed reactants.

A starting overall reaction involving $TiCl_4$ and C_2H_4 which could account for the formed intermediate reaction phase is

$$2TiCl_4 + C_2H_4 \rightarrow 2TiC + 4HCl + 2Cl_2 \quad (1)$$

as suggested by small quantities (3–5 at %) of chlorine contamination revealed by XPS in the as-synthesized powders.

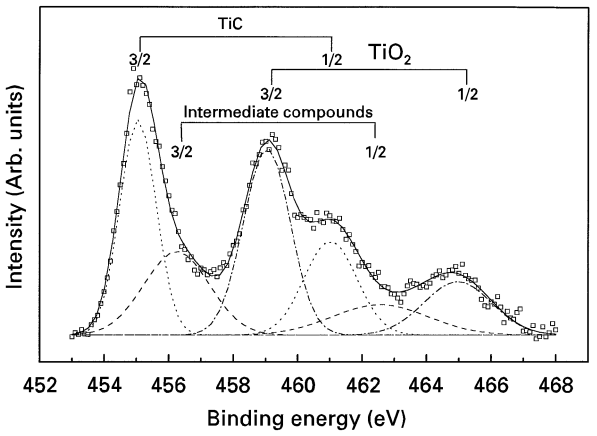

Figure 5 Decomposition of Ti 2p photoemission curve of TiC powder produced in run 0.

3.2. SiC/TiC synthesis

By adding a silane flow to $TiCl_4$ and hydrocarbons, a homogeneous mixture of SiC and TiC phases could be obtained. Table II gives the production parameters of Si/Ti/C composite powders, together with reactants depletion, weight percentages of the constituents, determined by chemical analysis and volume relative percentages of TiC and SiC phases, calculated from XRD patterns.

Analysis of the exhausted gases revealed an almost complete SiH_4 dissociation and the formation of various amounts of chlorosilanes (mainly $SiHCl_3$ and $SiCl_4$) which were also detected by Suzuki *et al.* in Si–H–Cl gas-phase systems below 1275 K [15].

As in the case of TiC powders, chemical and surface analyses evinced the extremely high reactivity of the SiC/TiC compound against oxygen. The formation of intermediate compounds prevented any direct quantitative estimate of the SiC and TiC content. Information could be gained from the XRD diffraction analysis due to its sensitivity to only the crystalline fraction of the powders. Assuming an amorphous structure of the mixed oxides, as observed in the TiC powders, the diffraction peaks (Fig. 6) could be reasonably ascribed to the contributions of crystalline SiC and TiC compounds. Silicon and titanium carbides possess both a cubic structure with comparable lattice parameter ($a = 0.46$ nm) and due to the reflection broadening coming from the nanosized dimensions, their contribution to the scattering intensity, overlapped indistinguishably. Fortunately the relative intensity of the (1 1 1) and (2 0 0) SiC peaks are different from those of (1 1 1) and (2 0 0) TiC, so that the relative percentage could be calculated with the help of standard patterns. X-ray diffraction also showed that SiC in the composite powder presented its low-temperature β-form, which, according to hot-pressing results [5] should be more favourable for the fabrication of SiC–TiC composites.

A qualitative description of the chemical reaction induced by laser heating could be derived from the comparison of Si *KLL* Auger spectra and of Si 2p,

TABLE II Experimental parameters for Si/Ti/C powder formation

Run	$TiCl_4$ (standard $cm^3\ min^{-1}$)	SiH_4 (standard $cm^3\ min^{-1}$)	C_2H_2 (standard $cm^3\ min^{-1}$)	C_2H_4 (standard $cm^3\ min^{-1}$)	P (torr)	T (°C)	Yeld ($g\ h^{-1}$)	$\frac{[SiH_4]_f}{[SiH_4]_i}$	$\frac{[C_2H_2]_f}{[C_2H_2]_i}$	$\frac{[C_2H_4]_f}{[C_2H_4]_i}$	Si (wt %)	Ti (wt %)	C (wt %)	O (wt %)	TiC (vol %)	SiC (vol %)
1	52	100	–	200	500	1250	24	0.005	–	0.28	26.6	39.0	28.5	5.9	36	64
2	52	100	250	–	400	1400	22	0.010	0.50	–	34.1	22.4	33.8	9.7	13	87
3	69	50	200	–	400	1540	12	0.040	0.75	–	6.7	37.6	44.2	11.5	50	50

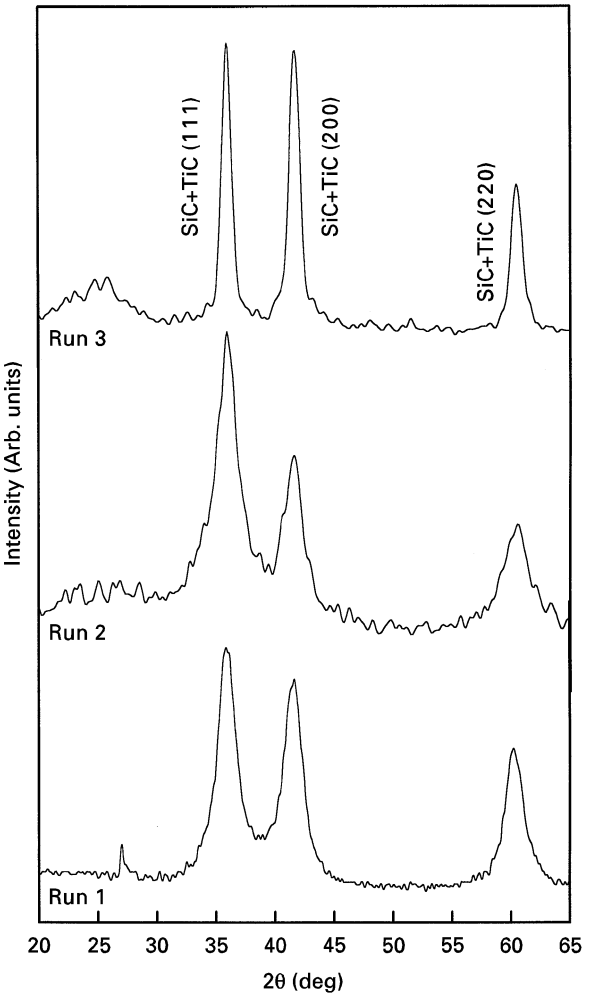

Figure 6 X-ray diffraction patterns of SiC/TiC powders produced according to parameters of Table II.

Ti 2p, and C 1s photoemission peaks recorded on the different SiC/TiC synthesized powders. Si *KLL* Auger spectra of the three runs are compared in Fig. 7. The main peak of samples 1 and 2 was ascribable to the Si–C bond. The different line shape observed on sample 3 showed an almost complete oxidation of the surface. The decomposition of the Si 2p peaks for samples 1 and 2, shown in Fig. 8, allowed more precise quantification of the relative proportion of silicon atoms engaged in bonds with oxygen and carbon [16]. The resulting atomic percentage of silicon bonded to carbon was 60% and 90% of the total silicon in samples 1 and 2 respectively, while the remaining silicon fraction could be attributed to Si–O bonds.

The photoemission Ti 2p measured on the same samples agreed with the previous results, showing a much higher oxidation degree even of the titanium atoms in sample 3.

XPS C 1s photoemission peaks, reported in Fig. 9, showed the simultaneous occurrence of unreacted carbon and carbides. The relative intensities of the signals attributed to C–Ti and C–Si bonds turned out to be in agreement with the trend of volumetric fractions of carbides calculated by XRD analysis.

Combining all the experimental results, it could be noticed that the laser process for producing SiC/TiC

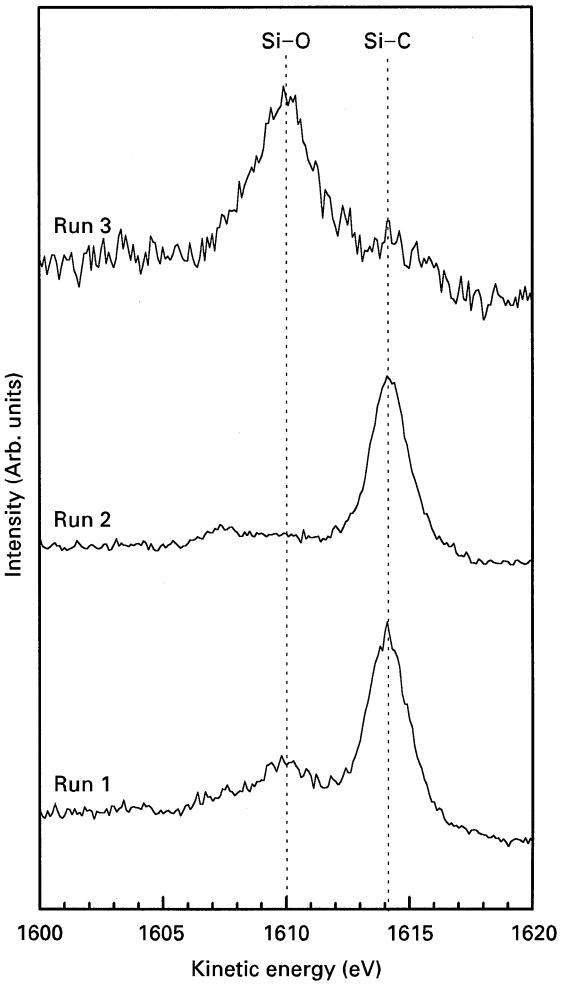

Figure 7 Si *KLL* X-ray induced Auger spectra of SiC/TiC composite powders.

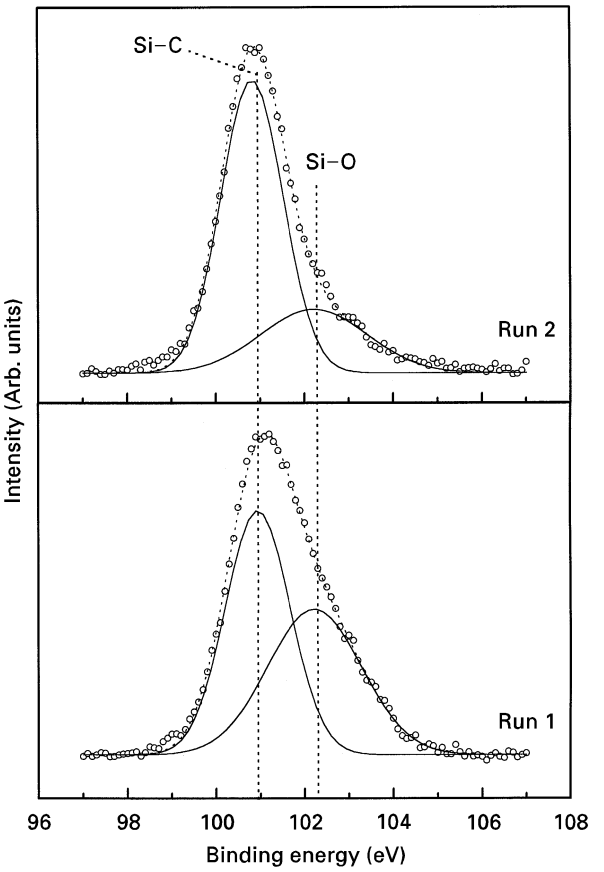

Figure 8 Decomposition of Si 2p photoemission peaks of SiC/TiC powders corresponding to runs 1 and 2.

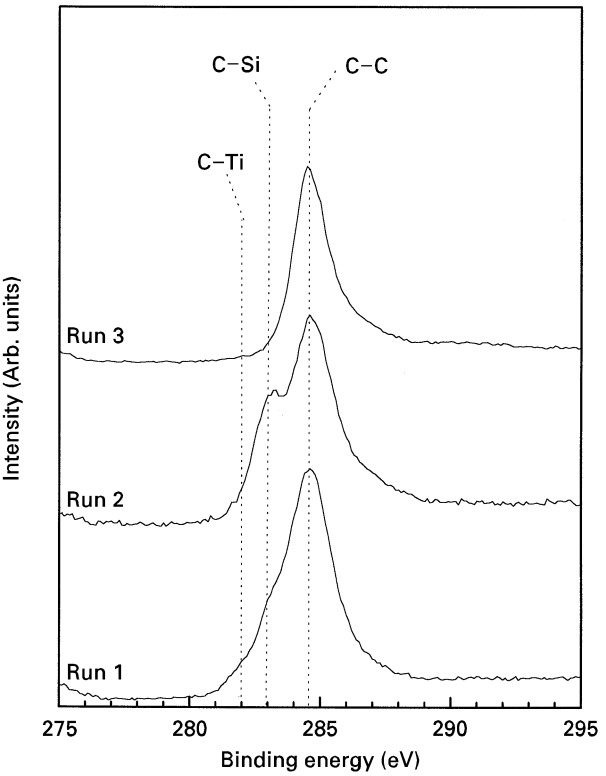

Figure 9 Comparison of the C 1s photoemission peaks for samples produced in runs 1, 2 and 3.

nanocomposite powders was more effective (yield 22–24 $g\,h^{-1}$) for SiC-rich compositions. The use of acetylene instead of ethylene as carbon precursor favoured the formation of the SiC phase as expected from the higher heat of formation measured for the laser-induced chemical reaction involving SiH_4 and C_2H_2 to form the SiC compound. Increasing the $TiCl_4/SiH_4$ ratio of the inlet reactants mixture led to an enrichment of the TiC phase of the synthesized powder, but it caused, in the mean time, a considerable lowering of the production yield and a consistent amount of unreacted carbon contamination of the powder. A mechanism similar to that described previously for TiC synthesis could be assumed. Although in this latter case the reaction process was surely more complex, owing to the presence of SiH_4 which simultaneously participated as reactant and as reaction sensitizer for $TiCl_4$, nevertheless it is reasonable to suppose that by increasing the $TiCl_4/SiH_4$ ratio, the chemical environment in the laser-heated region was closer to the synthesis of the single TiC phase.

As far as carbon contamination is concerned, it is of some interest to observe that a common trend characterized TiC and SiC/TiC nanoparticles synthesis: the larger the quantity of unbounded carbon found in the samples, the larger was the oxygen contamination after air exposure. Probably the pyrolitic amorphous carbon formed during the synthesis due to its huge specific area ($\sim 1000\,m^2\,g^{-1}$) might provide very active surface sites for oxygen adsorption as observed for the edge atoms of graphitic carbon [17].

4. Conclusion

The CO_2 laser-induced pyrolysis of $TiCl_4$, hydrocarbons and SiH_4 mixture, has proved to be a viable process for the synthesis of TiC and TiC/SiC nanoparticles. In particular, the production yield for powders composed of β-SiC matrix with the addition of up to 20% TiC phase is quite good. Both TiC and Si/Ti/C nanopowders are extremely reactive to the air exposure, thus requiring stabilization treatments before further processing. Research is in progress to overcome such limits.

References

1. K. NIIHARA, *J. Ceram. Soc. Jpn* **99** (1991) 10 974.
2. J. E. SUNDGREN and H. T. G. HENTZELL, *J. Vac. Sci. Technol.* **A4** (1986) 2259.
3. M. SRINIVASAN, in "Structural Ceramics", Treatise on Materials Science and Technology, Vol. 2, edited by B. Wachtman Jr, (Academic Press Inc., San Diego, California), p. 100.
4. K. W. CHAE, K. NIIHARA and D. Y. KIM, *J. Mater. Sci. Lett.* **14** (1995) 1332.
5. H. ENDO, M. UEKI and H. KUBO, *J. Mater. Sci.* **26** (1991) 3769.
6. J. S. HAGGERTY and H. K. BOWEN, MIT Report, Grant, NAG3-312 (1985).
7. R. W. CANNON, S. C. DANFORTH, J. H. FLINT, J. S. HAGGERTY and R. A. MARRA, *J. Am. Ceram. Soc.* **65** (1982) 324.
8. E. BORSELLA, R. FANTONI, S. PICCIRILLO, R. CECCATO and S. ENZO, *J. Mater. Res.* **5** (1990) 143.
9. E. BORSELLA, S. BOTTI, R. FANTONI, R. ALEXANDRESCU, I. MORJAN, C. POPESCU, T. DIKONIMOS MAKRIS, R. GIORGIO and S. ENZO, *ibid.* **7** (1992) 2257.
10. E. BORSELLA, S. BOTTI, R. ALEXANDRESCU, I. MORJAN, T. DIKONIMOS MAKRIS, R. GIORGIO and S. MARTELLI, *Mater. Sci. Eng.* **A168** (1993) 177.
11. M. S. HSU, M. A. MEYERS and A. BERKOWITZ, *Scripta Metall. Mater.* **32** (1995) 809
12. R. MACH, H. D. KLOTZ, F. OLESZAK, C. OLSCHEWSKI, I. DÖRFEL and K.-D. SUHRKE, in "Proceedings of the Fourth Euro Ceramics", Vol. I, edited by C. Galassi, (Gruppo Editoriale Faenza Editrice, Faenza, Italy, 1995) p. 89.
13. G. D. SORARU, A. GLISENTI, G. GRANOZZI, F. BABONNEAU and J. D. MACKENZIE, *J. Mater. Res.* **5** (1990) 1958.
14. C. LAVOIE, M. MEUNIER, S. BOIRIN, R. IZQUIERDO and P. DESJARDINS, *Appl. Phys. A* **53** (1991) 339.
15. M. SUZUKI, Y. NAKATA, T. OKURAMI and A. KATO, *J. Mater. Sci.* **27** (1992) 609.
16. R. GIORGI, S. TURTU, G. ZAPPA, E. BORSELLA, S. BOTTI, M. C. CESILE and S. MARTELLI, *Appl. Surf. Sci.* **93** (1996) 101.
17. H. WESTBERG, M. BOMAN and A. S. NOREKANS, *Thin Solid Films* **215** (1992) 126.

Received 25 October 1996
and accepted 17 April 1997